Remote Sens. **2015**, *7*, 2602-2626; doi:10.3390/rs70302602

OPEN ACCESS

remote sensing

ISSN 2072-4292

www.mdpi.com/journal/remotesensing

Article

Self-Adaptive Gradient-Based Thresholding Method for Coal Fire Detection Based on ASTER Data—Part 2, Validation and Sensitivity Analysis

Xiaomin Du [1,2], Sergio Bernardes [3,*], Daiyong Cao [1], Thomas R. Jordan [2], Zhen Yan [4], Guang Yang [1] and Zhipeng Li [5]

1 School of Geosciences and Surveying Engineering, China University of Mining and Technology, Beijing 100083, China; E-Mails: xiaomin@uga.edu (X.D.); cdy@cumtb.edu (D.C.); yg0817@163.com (G.Y.)

2 Center for Geospatial Research, Department of Geography, The University of Georgia, Athens, GA 30602, USA; E-Mail: tombob@uga.edu

3 Biospheric Sciences Laboratory, The National Aeronautics and Space Administration (NASA) Goddard Space Flight Center, Greenbelt, MD 20771, USA; E-Mail: sergio.bernardes@nasa.gov

4 Department of Statistics, The University of Georgia, Athens, GA 30602, USA; E-Mail: yzhead@uga.edu

5 College of Resources and Environment, The University of Chinese Academy of Sciences, Beijing 100049, China; E-Mail: lizhipeng428@gmail.com

* Author to whom correspondence should be addressed; E-Mail: sergio.bernardes@nasa.gov; Tel.: +1-301-614-6656; Fax: +1-301-614-6695.

Academic Editors: Richard Gloaguen and Prasad S. Thenkabail

Received: 9 July 2014 / Accepted: 17 February 2015 / Published: 5 March 2015

Abstract: The self-adaptive gradient-based thresholding (SAGBT) method is a simple non-interactive coal fire detection approach involving segmentation and a threshold identification algorithm that adapts to the spatial distribution of thermal features over a landscape. SAGBT detects coal fire using multispectral thermal images acquired by the Advanced Spaceborne Thermal Emission and Reflection Radiometer (ASTER) sensor. The method was detailed by our previous work "Self-Adaptive Gradient-Based Thresholding Method for Coal Fire Detection Based on ASTER Data—Part 1, Methodology". The current study evaluates the performance of SAGBT and validates its results by using ASTER thermal infrared (TIR) images and ground temperature data collected at the Wuda coalfield (China) during satellite overpass. We further analyzed algorithm performance by

using nighttime TIR images and images from different seasons. SAGBT-derived fires matched fire spots measured in the field with an average offset of 32.44 m and a matching rate of 70%–85%. Coal fire areas from TIR images generally agreed with coal-related anomalies from visible-near infrared (VNIR) images. Further, high-temperature pixels in the ASTER image matched observed coal fire areas, including the major extreme high-temperature regions derived from field samples. Finally, coal fires detected by daytime and by nighttime images were found to have similar spatial distributions, although fires differ in shape and size. Results included the stratification of our study site into two temperature groups (high and low temperature), using a fire boundary. We conclude that SAGBT can be successfully used for coal fire detection and analysis at our study site.

Keywords: thermal infrared remote sensing; spontaneous combustion of coal seam-validations; simultaneous field measurement; advanced spaceborne thermal emission and reflection radiometer (ASTER)

1. Introduction

Subsurface and surface coal fires have been widely linked to pollution and loss of coal resources [1], making the identification and mapping of burning coal areas a critical component in understanding coal fire contributions to environmental degradation and to the economy. The occurrence and spatial distribution of coal fires are a function of coal properties, including microstructure, chemical constituents, and minerals (e.g., particle sizes and surface areas, rank, petrography, and pyrites) [2]. In particular, Spontaneous Combustion of Coal Seams (SCCS) is promoted by three main coal properties (high sulfur content, high thickness and low metamorphic degree) [3]. Environmental conditions also play an important role in the distribution of SCCS, including atmospheric, geological and mining conditions (e.g., temperature, moisture, barometric pressure, oxygen concentration, bacteria, coal seams and surrounding strata, as well as mining operational methods, among others) [3]. This study delineates subsurface and surface coal fires and assumes that coal fire distribution is not spatially continuous due to the heterogeneous nature of coal fire properties and environmental conditions, including the distribution of oxygen conductive tunnels. In addition, because of fissures penetrating the sandstone (a poor thermal conductor), associated with the tendency of hot air to transport heat vertically more than horizontally, we further assume that temperature should decrease sharply near the boundaries of coal fire areas, as one moves away from their center. Our assumptions are consistent with previous work by [4], who observed attenuation to cold ground within two meters of the edge of fire regions.

Remote sensing provides data and methods to efficiently monitor burning coal areas, having multiple advantages over more expensive and laborious ground-based efforts involving subsurface hotspot identification [5,6]. For instance, thermal infrared (TIR) images acquired by orbital sensors over multiple dates have been used effectively for coal fire anomaly detection [7]. In our previous work [8], we delineated coal fire areas by using TIR images acquired by the Advanced Spaceborne Thermal Emission and Reflection Radiometer (ASTER) sensor. The study proposed the Self-Adaptive

Gradient-Based Thresholding method (SAGBT) and used the spatial variation of temperature (increases or decreases) over the landscape. SAGBT assumes that temperature variation becomes greater near the edge of a coal fire area, when compared to the center or outside of the fire area. The current study extends our previous investigation and evaluates SAGBT under different irradiation intensities by using simultaneous satellite-field observation campaigns on 27 March 2013, and on 22 June 2013. These dates represent the spring equinox and the summer solstice in the Northern Hemisphere, corresponding to medium and high levels of solar radiation intensity, respectively.

To understand the performance of SAGBT when identifying coal fire thermal patterns and separating anomalies, we spatially sampled temperature data using different strategies. Field campaigns collected land surface temperature in three blocks representing typical fire zones, six transects crossing coal fire areas and ten hotspots or fire boundary spots. These data were used with other records of temperature measurements and ASTER images to validate SAGBT in a variety of ways: (1) block samples were used with a hypothesis test; (2) temperature measurements along transects were compared with temperature profiles from ASTER; (3) measured coal fire spots were matched to coal fire areas to verify the accuracy of coal fire locations; (4) ASTER TIR-based coal fires were cross validated by using coal fires retrieved from visible-near infrared (VNIR) bands; (5) block samples were interpolated into fine-resolution images to validate high-temperature areas using coal fires from ASTER; and (6) coal fires were spatially compared, considering nighttime and daytime images acquired on the same date.

2. Materials and Data

2.1. Regional Geographical and Geological Overviews

The Wuda coalfield is an "ear-shaped" asymmetric syncline located in the western suburbs of Wuhai city, an industrial coal-mining city located in the Inner Mongolia Autonomous Region, China (upper part in Figure 1). The coalfield is bounded by the following coordinates: 39°28′21.15″N, 106°36′21.83″E, 39°34′6.01″N, 106°39′15.53″E and has elevations ranging from 1090 m to 1380 m above sea level. The area is located in the northern edge of the Helan Shan mountain range and is close to the Ulan Buh Desert. The climate of the area is arid. The field has three active coalmines, Suhaitu, Huangbaici, and Wuhushan, which are operated by the largest coal company in Wuhai, the Wuhai Energy Company (WEC).

The Wuda coalfield is a primary source of cooking coal in Northern China. The field consists of coal-bearing strata of the Pennsylvanian Taiyuan Formation (C_{3t}) in the Upper Carboniferous System; the Shanxi Formation (P_{1s}) in the Permian system; the Early Permian Xiashihezi (P_{1x}) formations, and the Late Permian Shangshihezi Formation (P_{2s}h). P_{1s} and C_{3t} are the major coal-bearing formations in the region, consisting of sandstone, limestone, mudstone, and mineable coal beds [9]. Five broad, stable, and minable coal seams, No. 1, 2, 4, 6 and 7, are located in P_{1s}, and coal seam No. 9 is in the coal-bearing stratum C_{3t} [10]. At the end of the Mesozoic era, due to the effect of Yanshan movement, a series of near north-south structure lines were formed parallel to the strata strike. Then, affected by the Cenozoic Himalayan orogeny, east-west tectonic lines cut off the structure lines perpendicularly. These latter movements created the fissures observed in the coalfields. Figure 1 (bottom) presents a

geological section of the area, showing the coalfield situated in an asymmetric syncline basin with relative flat west wing and steep east wing that was cut by a nearly 9 km length over-thrust fault [10]. Strata in the northern part of this basin have a NE-SW strike direction and are flatter and wider than those found in the southern part [9]. The lowest coal seam outcrop (Figure 1a) and the over-thrust fault line (Figure 1b) enclose the outer boundary of the coalfield on the surface. Underneath this area, there are coal-bearing strata (Figure 1c), and the area is considered a fire risk. Coal fires in Wuda are accompanied by features on the surface, such as large-scale oxygen conductive tunnels (cracks and vents, Figure 1d), coal tar precipitation spots (Figure 1e) and released smoke/steam (Figure 1f). Some waste laneways (Figure 1g) also form oxygen conductive tunnels.

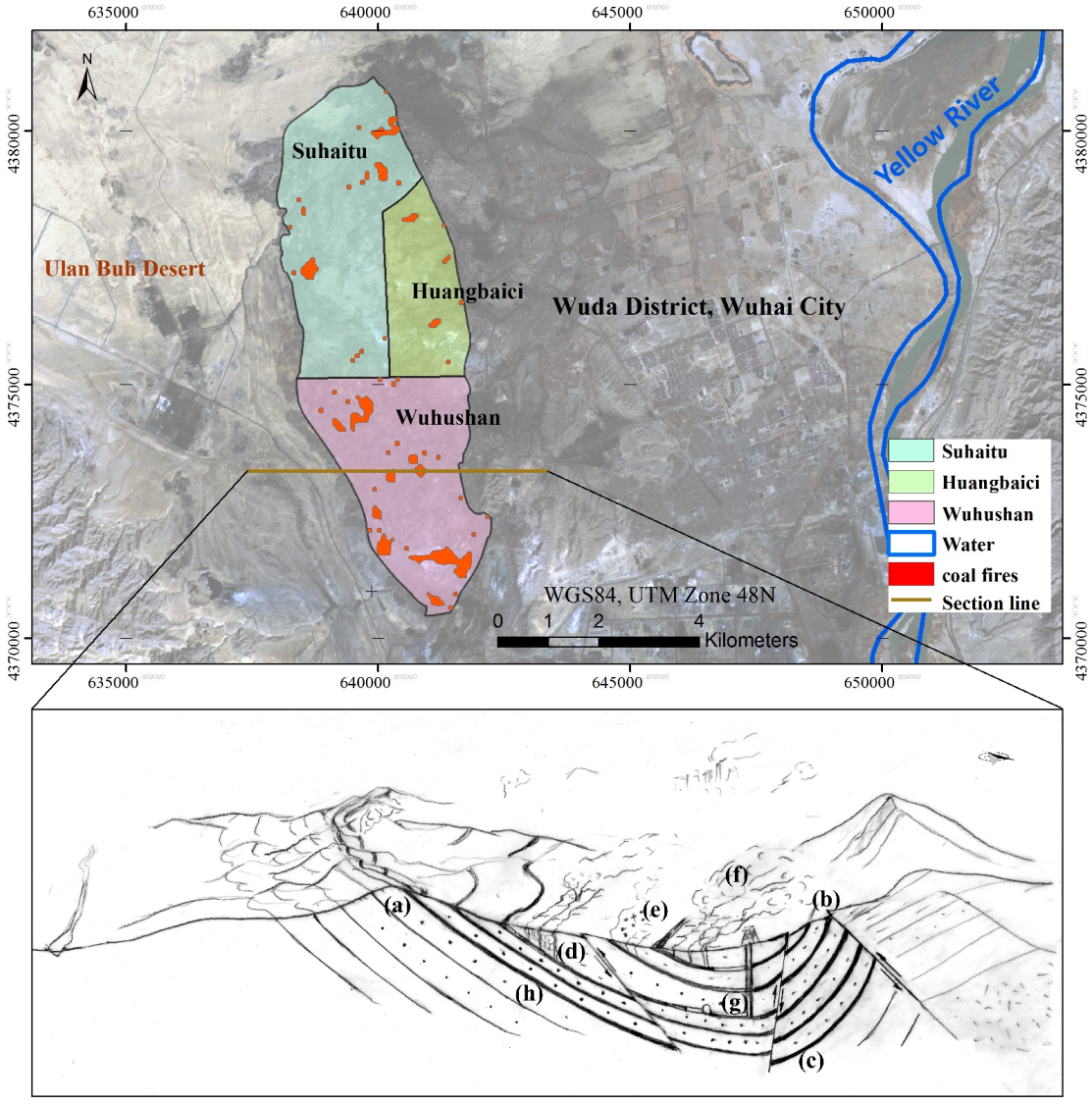

Figure 1. Location of the study area (Wuda coal field) and geology of the field. Top: coal fires are shown for three active coalmines in the field with coal fire polygons (red) depicting fires for 22:58 22 June 2013, mapped using self-adaptive gradient-based thresholding (SAGBT) (local time = UTC + 8); Bottom: east-west geological section along the southern part of the field and including: (**a**) coal seam outcrops; (**b**) thrust fault line; (**c**) coal seams; (**d**) cracks and vents; (**e**) coal tar precipitation spots; (**f**) mining laneway system; (**g**) smoke and steam; and (**h**) sandstone.

2.2. Land Use and Land Cover

The study area encompasses relatively homogeneous, wind eroded sands and coal dust, which are widely distributed over the region. Work by [5] produced a classification of the Wuda coalfield and its surrounding area into 12 land cover classes. Then, we used the constraint of the coalfield boundary, and several non-vegetation classes (e.g., sandstone, limestone, metamorphic, mixed sandstone with shale, coal and coal dust, bare land, and Gobi desert) were included in the ear-shaped syncline. Values of the Normalized Difference Vegetation Index (NDVI) derived from ASTER images acquired on 22 June 2013 (summer solstice) indicate reduced vegetation (mean = −0.13; max = 0.25; standard deviation = 0.02). NDVI calculated for other seasons confirms these results: 27 March 2013 (mean = −0.09; max = 0.05; standard deviation = 0.01); 26 September 2013 (mean = −0.09; max = 0.25; standard deviation = 0.02); and 23 December 2013 (mean = 0.02; max = 0.07; standard deviation = 0.01). The Wuda field has very sparse vegetation, resulting in an almost bare landscape. The reduced vegetation cover creates ideal conditions for coal fire detection using the spatial variability of ground temperature.

2.3. Thermal Remote Sensing Data

We used nine 90-m resolution TIR bands from ASTER (bands 10 to 14, from 8.125 to 11.65 μm) as input to a temperature emissivity separation, maximum minimum difference method (TES-MMD) [11]. TES-MMD was used to retrieve temperature and spectral emissivity during coal fire detection and validation and included the processing of nine ASTER Level-1B scenes (Table 1), acquired on 21 September 2002; 29 November 2007; 26 March 2010; 27 March 2013; 22 June 2013; and on 26 September 2013.

Table 1. ASTER and Landsat 8 data used in this study, including acquisition date and period of acquisition (day or night).

Sensor	Date and Time of Acquisition (Time is Local Time = UTC + 8)	Day/Night
ASTER	22:54:22 21 September 2002	Night
	11:54:17 29 November 2007	Day
	22:58:56 29 November 2007	Night
	11:54:35 26 March 2010	Day
	11:48:38 27 March 2013	Day
	22:53:17 27 March 2013	Night
	11:54:43 22 June 2013	Day
	22:59:22 22 June 2013	Night
	11:54:34 26 September 2013	Day
TIRS (Landsat 8)	22:38:14 23 December 2013	Day

In addition, 15-m resolution VNIR bands from ASTER were used to compute NDVI; to identify coal fires using a false color composite, and to geocorrect the spatially coarser TIR bands. TIR bands are acquired during daytime and nighttime, as opposed to VNIR bands that are acquired only during the day. We used day/night image pairs for 27 March 2013, and 22 June 2013 with data measured in the field to verify our fire detection method. Nighttime images acquired on 27 March 2013 and on

22 June 2013 were used as cross validation scenes for daytime coal fire areas. An additional image pair acquired on 29 November 2007 was used to compare daytime and nighttime results during winter. Three ASTER VNIR scenes for 27 March 2013, 22 June 2013 and 26 September 2013 and one scene from Landsat 8 VNIR bands for 23 December 2013 were used to calculate NDVI for spring, summer, fall and winter. SAGBT validation also included one thermal image from Landsat 8 TIRS sensor, acquired on 23 December 2013. TIRS has two thermal infrared bands (10.3–11.3 μm and 11.5–12.5 μm) and has spatial resolution (100 m) similar to ASTER TIR bands. ASTER images acquired on 21 September 2002 and on 26 March 2010 were used as cross validation scenes for coal fire areas from other coal fire detection methods.

2.4. Field Data

Ground control point (GCP) collection in Wuda used a GPS receiver and considered coordinate acquisition at regular time intervals; at road intersections; bridges; and land use boundaries. GCPs were later used as reference during image geocorrection and during the spatial matching of VNIR and TIR images. The horizontal accuracy of GPS (<10 m) was considered to be adequate for this application. A handheld thermal infrared thermometer was used with the GPS receiver to collect more than 600 land surface temperature (LST) samples over the Wuda field.

3. Methods

3.1. Geometric Correction

Positional mismatches occur between images acquired at different dates/times, resulting from changes in satellite track and attitude, rectification algorithms and resampling procedures. We observed a 2-pixel to 5-pixel registration offset (90 to 450 m on the ground) for the ASTER images analyzed and registered images to GPS coordinates to allow for image overlay and analysis. To match TIR images to GPS points we used a two-step geocorrection approach, which included image-to-map and image-to-image registration. During image-to-map registration, VNIR images were geocorrected using GPS tracking points for the Wuda coalfield and for Wuhai city, as well as GCPs representing street corners and intersections. We then super-sampled TIR images to VNIR spatial resolution and used an image-to-image approach to register super-sampled TIR images to VNIR images. During registration, we used stream crossings, river islands, and industrial chimneys as GCPs. Figure 2 shows the distribution of GCPs used by these two registration strategies.

Nearest neighbor interpolation was used for image resampling to minimize changes in the original radiation values. Following the two-step geocorrection procedure, we registered the TIR images to VNIR images (average RMSE = 25.78 m, Table 2) and registered the VNIR image to GPS points (RMSE = 31.29 m, Table 3). These average errors correspond to less than 50% (45 m) of the spatial resolution of the TIR images.

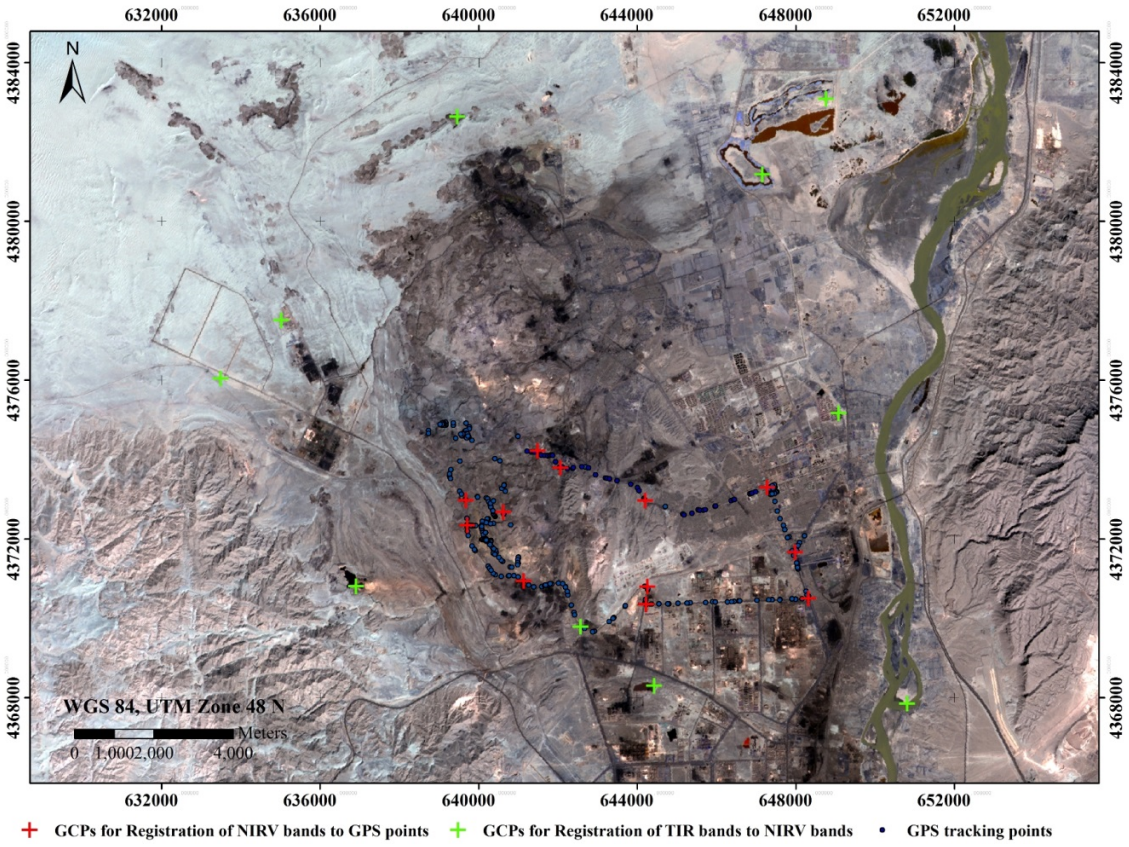

Figure 2. Ground control points (GCPs) selection during geometric correction. Green crosses are GCPs used in the registration of TIR to VNIR images (points have stable and high temperature contrast). Red crosses mark the GCPs used for registration of VNIR images to GPS data (points were selected at intersections or at street corners). Linked blue dots are GPS tracking points.

Table 2. Error values for TIR to VNIR images registration.

Sensor	Date and Time of Acquisition (Time is Local Time = UTC + 8)	Day/Night	Error (m)
ASTER	11:48:38 March 27, 2013	Day	14.85
	22:53:17 March 27, 2013	Night	64.36
	11:54:43 June 22, 2013	Day	-- [1]
	22:59:22 June 22, 2013	Night	23.92

[1] This VNIR image matches the TIR image accurately. Thus, no geo-registration was applied.

Table 3. Error values for VNIR images to GPS points registration.

Sensor	Date and Time of Acquisition (time is local time = UTC +8)	Day/Night	Error (m)
ASTER	11:48:38 27 March 2013	Day	29.21
	11:54:43 22 June 2013	Day	33.37

3.2. Coal Fire Detection

We used five ASTER TIR bands as input to a TES-MMD algorithm, which has been demonstrated to produce 90-m spatial resolution temperature images (Figure 3a) with inversion error of 0.3 K [11]. Resulting temperature images were used with our gradient thresholding coal fire detection method to

identify surface temperature gradients, assuming the rapid decrease of LST towards the edge of a coal fire. This identification of extreme temperature gradient pixels and the connection of these pixels in space are key workflow elements for the delineation of coal fire areas. The use of ASTER TIR scenes acquired during different seasons precludes the use of a fixed threshold for segmenting temperature images. We previously addressed this limitation and proposed a method (SAGBT) that can be applied to multiple ASTER TIR scenes in a consistent and uniform way [8]. SAGBT defines coal fire areas as regions with temperature anomalies bounded by sharp decreases in LST, from central high temperature anomalies to low background temperature. The algorithm flags coal fire pixels with temperature greater than a threshold, calculated as the mean temperature of extreme gradient points (green, orange and red pixels in Figure 3b). Redundant potential high temperature buffers limited by temperature values greater than 1.0 σ from the mean are later created to prevent cold temperatures from being flagged (false positives) in relatively cold areas. Next, considering the gradient image, one pair of segmented bounds, a lower bound in the range of 0.5 σ–1.0 σ and an upper bound 3.2 σ, for an extremely high gradients image are considered as a potential boundary image for coal fires. Then, a thinning morphological operation skeletonizes extremely high gradients into a binary image with one-pixel wide extreme gradient lines (blue lines in Figure 3c). We observed that these extreme gradient lines maintain topological properties and connect high gradient pixels in the gradient image and surrounding high temperature areas in the temperature image. Masked within the fire risk area that is closed by the outer boundaries of the coal-bearing strata, an intermediate threshold was retrieved by reading an average temperature along the thinned extremely high gradient lines from the potential high temperature image (high temperature image showed in Figure 3a) [8].

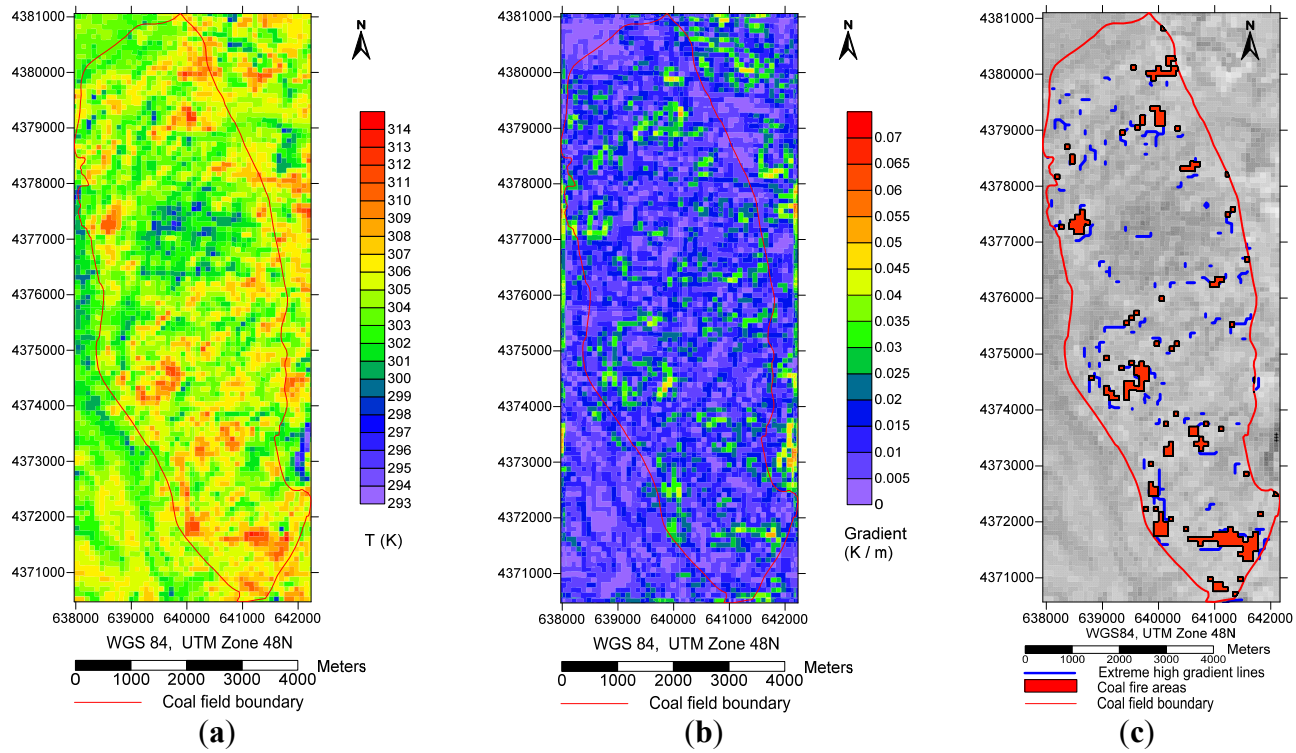

Figure 3. Gradient-based thresholding method, (**a**) daytime temperature image for 27 March 2013; (**b**) gradient image generated by an extended Sobel filter; (**c**) thinned extreme gradient lines (blue lines) and coal fire areas (red pixels) segmented by the final threshold.

In the fine-tuning process, the final threshold was selected as the mean value of multiple intermediate thresholds generated by eleven line sequences resulting from thinned extreme gradient images. These sequences were generated by changing the lower segment bounds of the extremely high gradient images from 0.5 σ to 1.5 σ (step = 0.1 σ). We observed stability in intermediate threshold values when extremely high gradient images changed, resulting in stable coal fire areas despite significant variation in binary images of extreme gradient lines. This final temperature is used to isolate coal fire areas. SAGBT is mainly based on the thermal spatial distribution of a TIR image itself. Figure 4 shows a coal fire map resulting from the method above and depicting coal seam outcrops and coalfield borders [8].

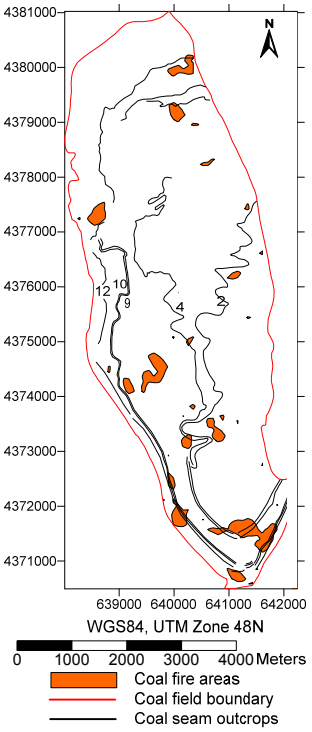

Figure 4. Coal fires extracted by our self-adaptive gradient-based thresholding (SAGBT) method mapped with coal seam outcrops. Orange areas indicate daytime coal fires for 27 March 2013. Black lines are coal seam outcrops.

3.3. Experiment Design and Validation Strategy

We tasked the ASTER sensor and acquired two pairs of daytime/nighttime cloud-free images over the study area. Images were acquired on days field surveys were carried out. Method validation used three strategies for field data collection, which included: (a) visually identified coal fire-induced hot spots (open burning coal seams, hot cracks/vents, and burning coal waste piles); (b) transect lines throughout the coal fire area; and (c) intense sampling block areas. We sampled 34 fire initiation sites (Figure 5, star symbol), aiming to verify the accuracy of SAGBT-derived coal fire locations. Measurements included six transects longer than 200 m (crossing more than three pixels) that extended across the burning area and represented individual fires (Figure 5, upper right window). Temperatures were measured at 25 to 30-m intervals and were later used to generate a temperature profile for validating SAGBT results. Intensive sampling was conducted on three dates, as shown by Figure 5: 6 October 2012 (block A, with

blue dots), 27 March 2013 (block B, with green dots) and 22 June 2013 (block C, with orange dots). Data collection for block A included intensive sampling along lines following an east-west orientation. In block B, three sub-blocks wider than 200 m were selected to represent burning areas, transitional areas, and background areas. In these sub-blocks, LST was measured in regular grids. In block C, only two sub-blocks were defined (burning area and background) due to difficulties in discriminating the transitional area. Due to unsafe conditions and lack of field personnel on 22 June 2013, data were collected in an approximate zigzag pattern over the sampling area. Temperature and coordinates recorded for every sampling block were used to generate fine resolution temperature images to validate the high-temperature relatively coarser pixels from ASTER. Samples were also used to test the hypothesis that temperatures in the delineated fire areas were warmer than background temperatures, for images acquired on 27 March and on 22 June 2013. In addition, we assessed the delineation of coal fires derived from daytime and nighttime ASTER TIR images, and compared coal fire induced thermal patterns identified by using ASTER TIR and VNIR images.

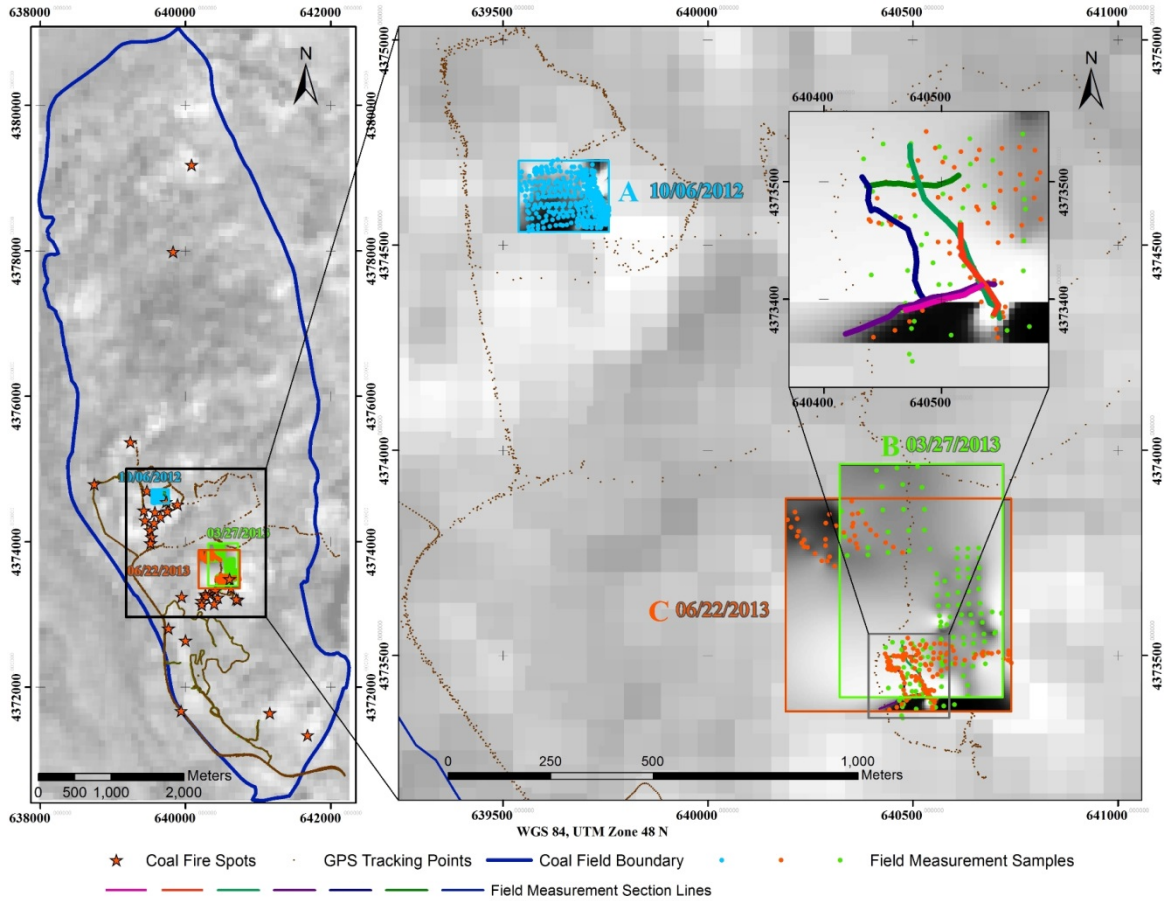

Figure 5. Field measurement strategies including three blocks and six sampling lines. Field surveys were conducted on 6 October 2012 (block A, blue dots), 27 March 2013 (block B, green dots), and 22 June 2013 (block C, orange dots). Blocks A, B and C included burning areas, coal fire edges, transitional areas and background.

4. Results and Discussion

4.1. Hypothesis Test Result

To test the accuracy of coal fire delineation by SAGBT, we analyzed 256 temperature measurements collected at our sampling blocks. Our null hypothesis was that temperatures inside a coal fire area are not significantly higher than the temperatures outside the area. Considering the size of our sampling population, we assumed that measurements inside (group 1) and outside (group 2) coal fire areas were normally distributed. We then used Student's *t*-test to determine whether these data groups were significantly different from each other. Figure 6 shows the spatial distribution of points tagged as high temperature (group 1) or low temperature (group 2) by SAGBT. Two sets of samples were analyzed, corresponding to two different dates: 27 March 2013 (spring) and 22 June 2013 (summer). Coal fires retrieved from nighttime and daytime images were used to further divide the samples into high and low temperature groups.

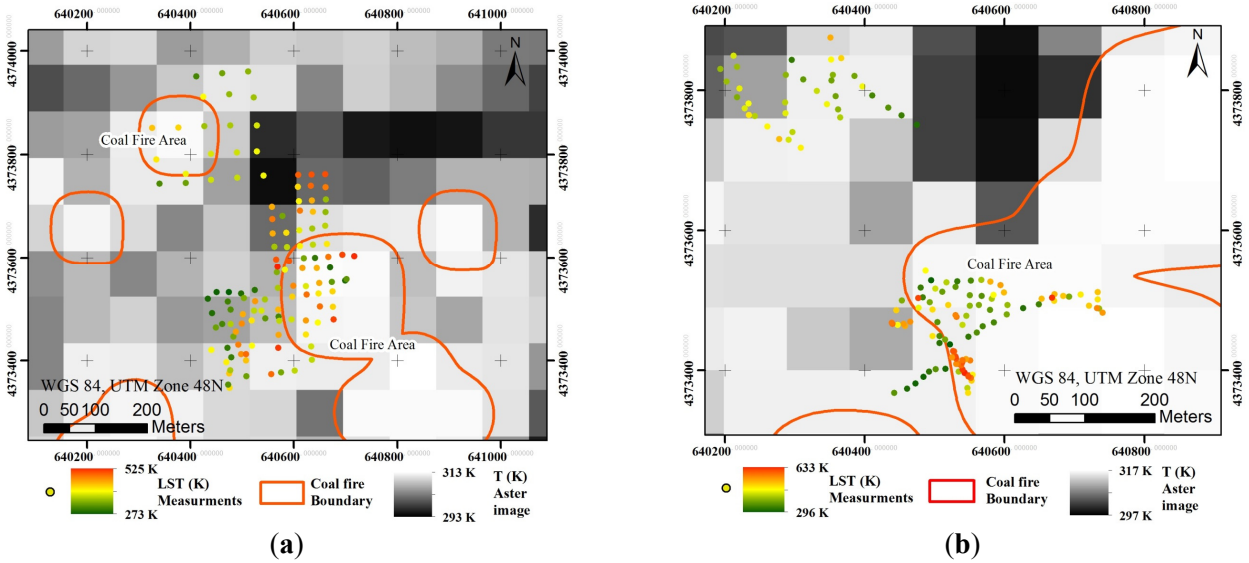

Figure 6. Hypothesis testing layout showing sets of points from (**a**) 27 March 2013 and (**b**) 22 June 2013. Points were measured inside the coal fire area (high temperature group) and outside the fire area (low temperature group).

No significant difference was found for distribution variances of the two groups and dates considered (significance level = 0.05). A test of temperature differences by using the "pooled" method with the *t*-test showed that the null hypothesis was rejected for the March and the June sets (Table 4). It is noteworthy that, when using nighttime coal fire boundaries, two groups (inside and outside of coal fires) were observed to have a larger difference in mean temperatures. Additionally, confidence intervals are less overlapping for the March and June data sets (95% CI in Table 4).

Histograms of LST (Figure 7) indicate that normality can be assumed for groups of field temperature measurements segmented by daytime fires and by nighttime fires. In addition, low and high temperature groups show different mean values, indicating that SAGBT can separate coal fire areas from cold background. Coal fires retrieved from nighttime images allowed for better separation of samples into

high and low temperature groups, as shown by the *t*-test results. A two-way analysis of variance (not shown) also revealed that the use of nighttime images significantly affects coal fire delineation.

Table 4. Hypothesis test output.

Season	Day/Night	Area	*N*	Mean	Std Dev	95% CI	*t*-test Results		
							DF	*t* Value	*Pr* > |*t*|
Spring (27 March 2013)	Day	high	36	299.7	6.5983	(297.4, 301.9)	118	1.47	0.144
		low	84	297.8	6.555	(296.3, 299.2)			
	Night	high	63	300.2	6.1205	(308.1, 315.3)	118	3.41	0.0009
		low	57	296.3	6.5394	(305.7, 310.4)			
Summer (22 June 2013)	Day	high	57	311.7	13.7217	(308.1, 315.3)	113	1.68	0.0964
		low	58	308.1	9.0240	(305.7, 310.4)			
	Night	high	34	313.9	11.9453	(309.8, 318.1)	114	2.48	0.0146
		low	82	308.2	11.1441	(305.7, 310.6)			

Surface temperatures measured along six transects in the field were compared to temperatures from the corresponding pixels from temperature images. Figure 8 shows the spatial arrangement of those transects and their IDs.

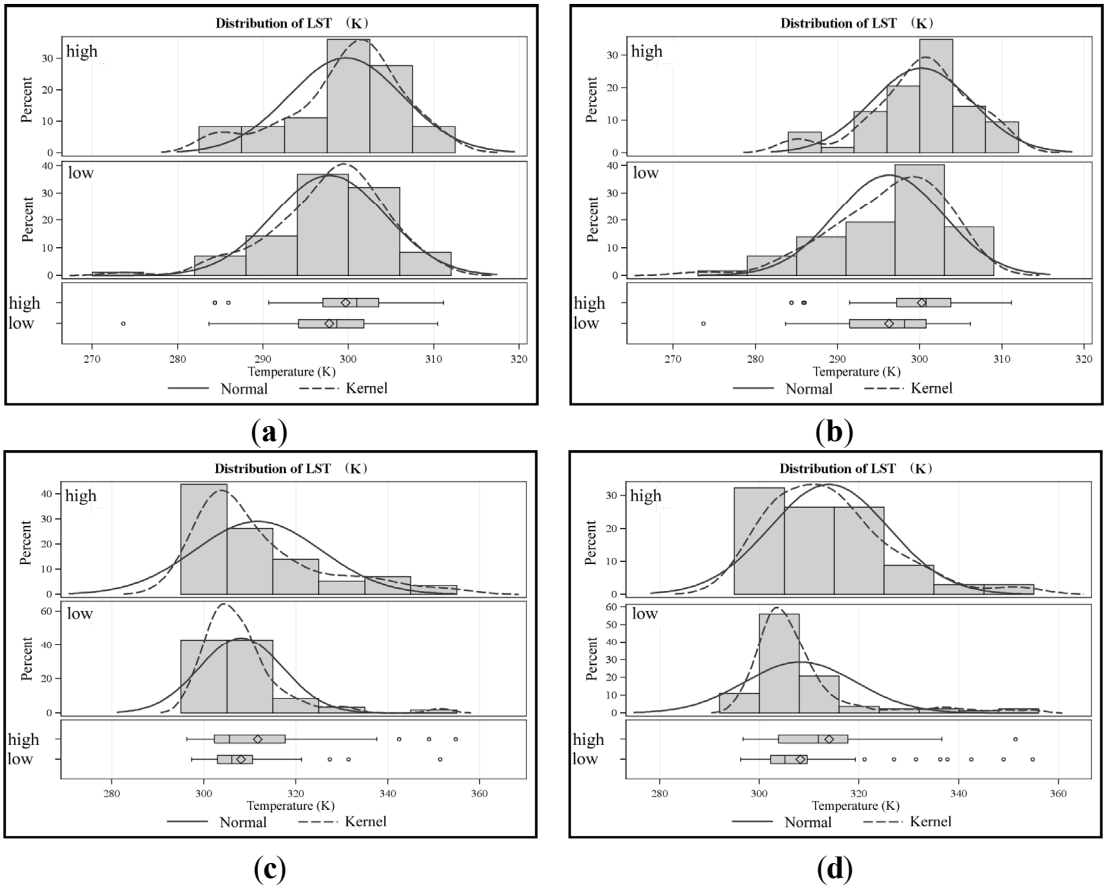

Figure 7. Distribution of temperature points for sets: (**a**) March (daytime); (**b**) March (nighttime); (**c**) June (daytime); and (**d**) June (nighttime). Points inside coal fire areas were identified as high-temperature. Points outside the fire area were identified as having low temperature.

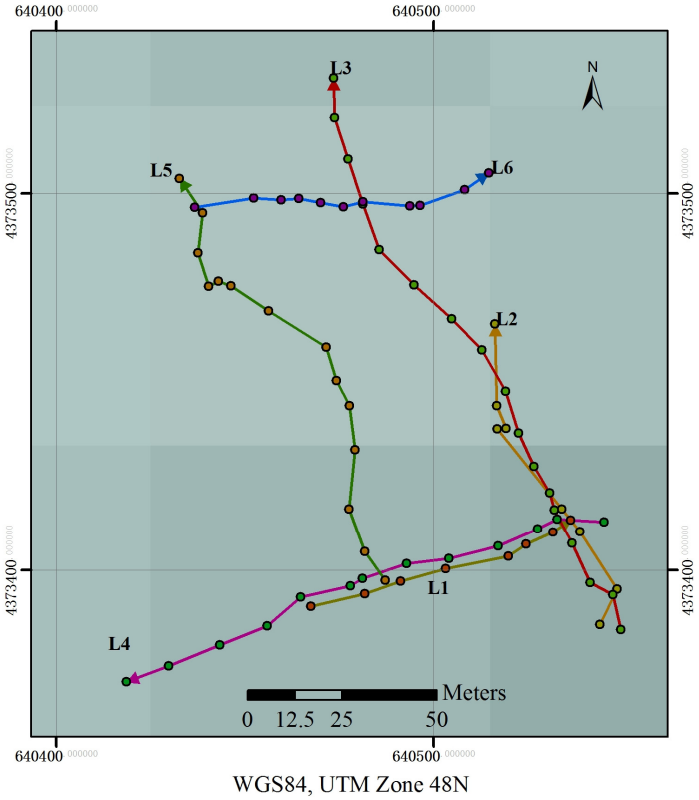

Figure 8. Spatial arrangement of six temperature-sampling transects measured on 27 March 2013 (L1 and L2) and on 22 June 2013 (L3, L4, L5 and L6). Circles are measurement locations. ASTER TIR pixels are shown in the background.

4.2. Comparisons Along Transects

Figure 9 shows temperatures sampled along field transects and from ASTER TIR images. All plots in Figure 9a–f show larger fluctuations in measured temperature, compared to image-based profiles. Because pixel values result from the integration of energy traveling within the field of view of the sensor, we expected relatively reduced variability in LST from remote sensing at this spatial resolution.

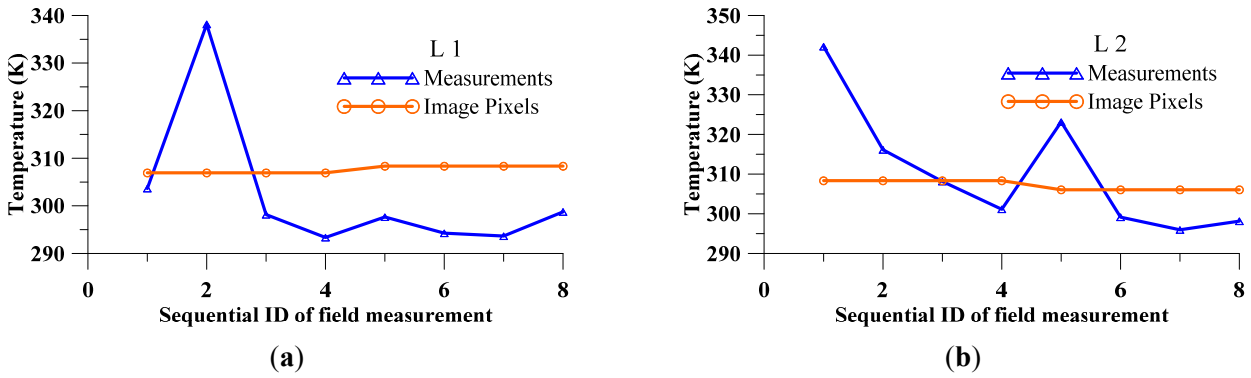

Figure 9. *Cont.*

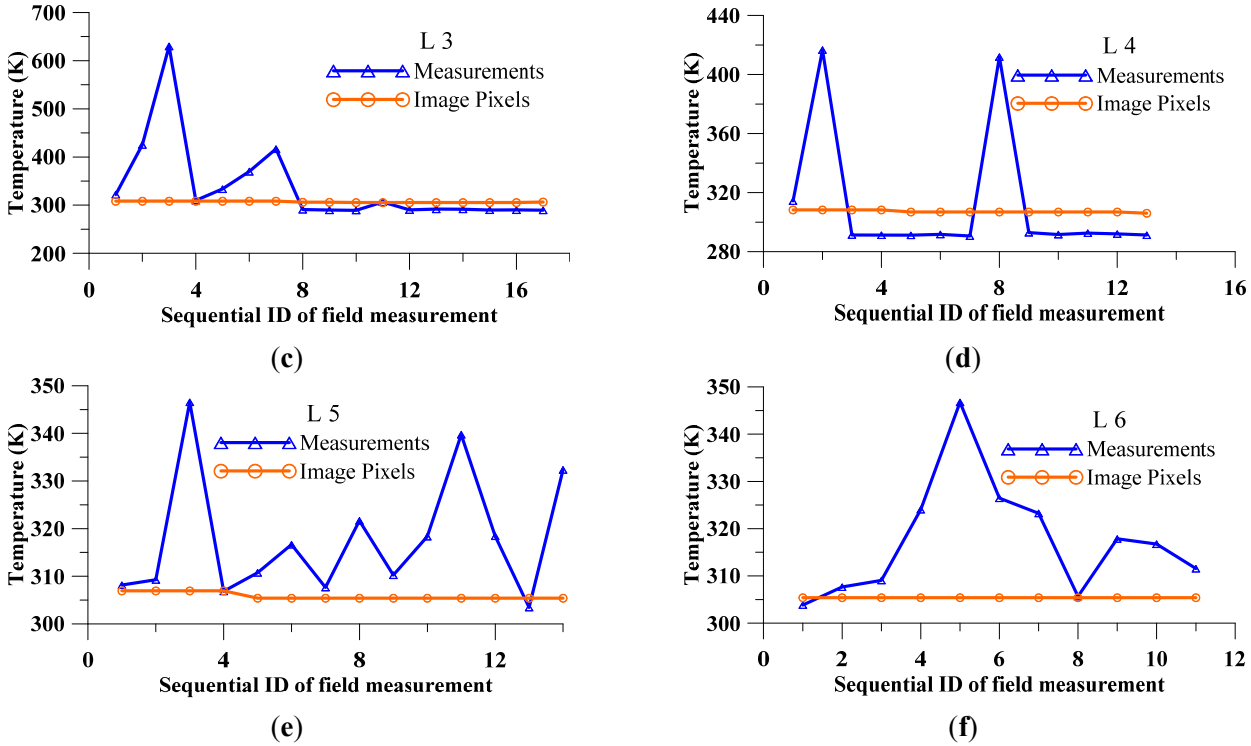

Figure 9. (**a**–**b**) Profiles of surface temperature values measured along transects (blue) and calculated from images (orange). Note: scale changes between graphs.

4.3. Comparisons between Measured Fire Spots and Coal Fire Areas

Sixteen fire spots measured on March 2013 were overlaid to coal fire areas identified by SAGBT (Figure 10a). A temperature image resulting from solar irradiation removal (DEM source: ASTER, 15 m resolution) is shown as background. Eleven fire spots (68.75% of total) matched fire areas from SAGBT (blue crosses in Figure 10a). A proximity analysis showed that 87.5% of the measured fire spots are within one pixel from SAGBT coal fires, including three of the mismatched spots in the southern part of the coalfield. Outside spots near coal fire areas may indicate that these are scattered fires or fires in the process of being extinguished. The two other mismatches (one located at the center sandstone plateau in the northern part of the coalfield and the other adjacent to coal fires) were tagged as missed fire spots. Results indicate that SAGBT can miss small fire spots that are not large, nor hot enough to create enough contrast between the fire pixel and its surrounding pixels (background).

For cross validation, we used SAGBT with a subset of a Landsat 8 TIRS scene corrected for solar irradiation. A comparison between output fire areas and measured fires (Figure 10b) showed that the majority (82.9%) of fire spots were within one pixel from fire areas. Exceptions were four fire spots adjacent to fire areas and two missed fires, including a spot over the center sandstone plateau in the northern part of the image subset. We assumed that due to the near axial part of the syncline the overlaid thick strata insulates heat from deep burning layers, although small hot spots can be observed at some coal fire vents.

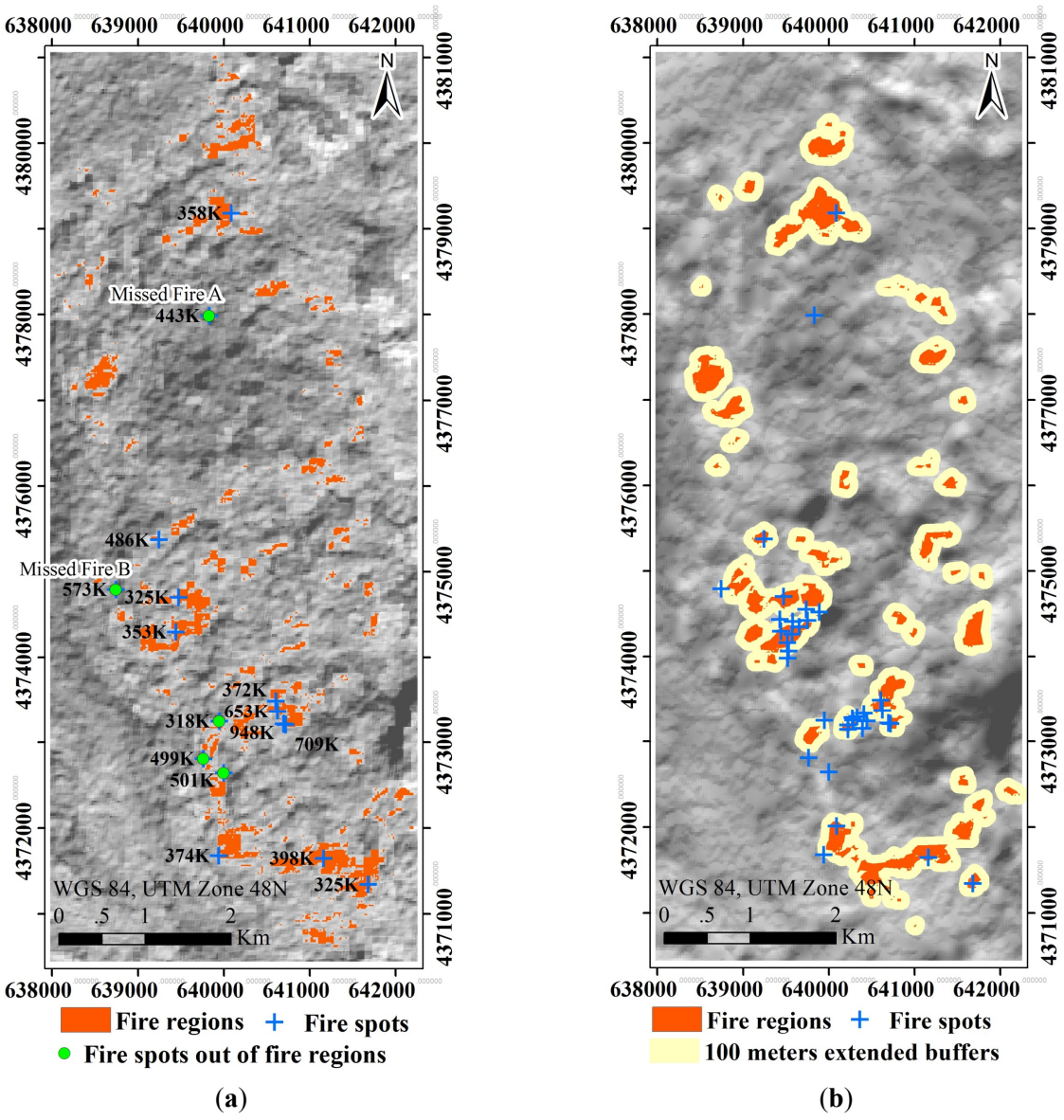

Figure 10. Spatial distribution of measured fire spots (blue crosses and green circles) and coal fire areas (orange) from our self-adaptive gradient-based thresholding (SAGBT) method. Blue crosses are matches between fire spots and fire areas. Green circles indicate fire spots in the proximity of fire areas. Temperatures (K) are presented for each spot. (**a**) Coal fires extracted from ASTER TIR image acquired on 27 March 2013; (**b**) Coal fires extracted from Landsat 8 TIRS acquired on 23 December 2013.

A field survey in July 2013 identified landscape features indicative of fire boundaries (e.g., edges of coal waste piles and outcrops in the coal fire area). Figure 11 shows that these boundaries (blue crosses) were close to fire areas or were on the edge of fire areas, as identified by SAGBT (ASTER TIR images from 22 June 2013). The average distance between fire spots and their nearest retrieved fire boundary (32.44 m) is less than one TIR pixel (90 m), supporting the conclusion that the offset between detectable coal fire boundaries and the retrieved fire area is less than the resolution of an ASTER image.

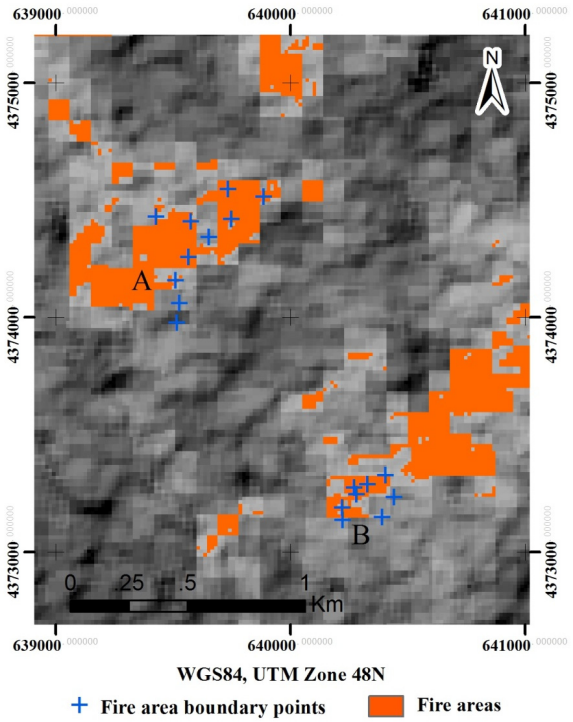

Figure 11. Locations of landscape features indicative of coal fire boundaries (blue crosses) and coal fire areas (orange) from our self-adaptive gradient-based thresholding (SAGBT) method. ASTER TIR image (22 June 2013) is used as background.

4.4. Comparisons between Optical Images and Coal Fire Areas

In addition to temperature, other landscape features are associated with coal fire areas and can be visually detected, including coal tar precipitation spots, fissures, burnt rocks and locations where fire extinguishing practices have been conducted. These features offer additional opportunities to validate SAGBT using optical bands. Figure 12 depicts coal fire areas in Wuda (Figure 12a,b), as well as results of coal fire detection using TIR overlaid to ASTER VNIR (15 m), both acquired during daytime.

(a) **(b)**

Figure 12. *Cont.*

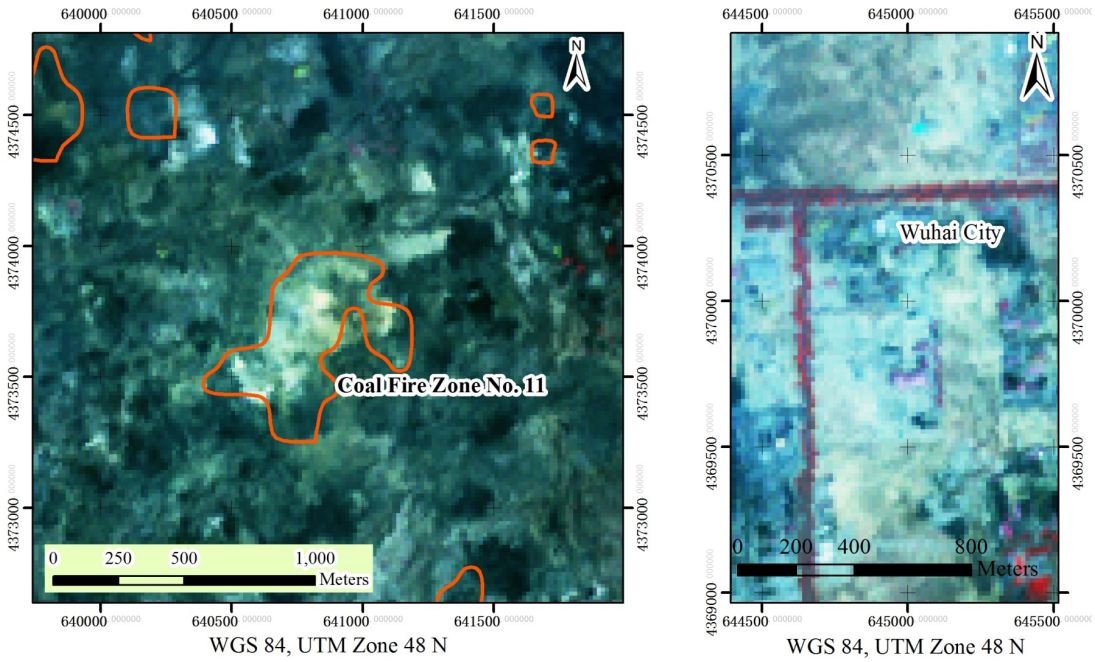

Figure 12. Ground and orbital views of areas affected by fire in the Wuda field: (**a**) excavation area for fire extinguishing in Coal Fire Zone No. 11; (**b**) excavated coal fire area in Coal Fire Zone No. 11; (**c**) Coal Fire Zone No. 11 (center polygon), overlaid to a high-reflectance area, as shown by ASTER VNIR; (**d**) similarities in spectral responses between a coal fire extinguishing area and a residential area in Wuhai city.

High reflectance areas (light areas) delineated by coal fire polygons likely result from rocks that were recently exposed due to fire extinguishing operations involving explosions and excavations (Figure 12a). Work to extinguish fires results in large areas of excavated and exposed rocks (Figure 12b) and these areas are shown as light tones by ASTER VNIR (Figure 12c). Reflectance values for these areas are similar to those observed for residential areas and concrete buildings in Wuhai city (Figure 12d). Conversely, low reflectance areas (dark areas) indicate coal waste piles or opencast mining areas. Fire occurrence in coal waste piles has been widely reported in the Wuda field.

4.5. Comparison between Interpolated High-Resolution Thermal Images and Coal Fire Areas Retrieved from ASTER

Field temperatures from 6 October 2012 and field temperatures collected during an ASTER overpass in 2013 were interpolated to create two-meter resolution images. The interpolated images were masked using boundaries of sampling blocks and the resulting surfaces were compared to coal fire areas identified using ASTER daytime collections from 27 March 2013 and from 22 June 2013.

We have previously observed that SAGBT-derived coal fire areas match high-temperature pixels in ASTER images, and that these areas include major high-temperature regions from field samples. Figure 13a shows general agreement between coal fire boundaries (polygon lines) from SAGBT and high-temperatures from an interpolated surface. A stronger match is observed for thermal anomalies in the northwest of the region. In Figure 13b, a fire boundary crosses a transitional area with a sharp decrease in

temperature. Most of the high-temperature centers are encompassed or crossed by coal fire boundaries, except for a western center in Figure 13b. Thermal anomalies from field measurements collected approximately six months before image acquisition (27 March 2013) share similarities in the spatial distribution of coal fires and show strong heat in the east and northwest (Figure 13c). Past measurements were used to investigate changes in the study area and to test the sensitivity of SAGBT to those changes. Despite the six-month difference between field data acquisition and image collection, we observed that sampling points matched the coal fire area retrieved from the ASTER image on 27 March 2013. Results revealed that coal fire in the area was relatively stable during that period.

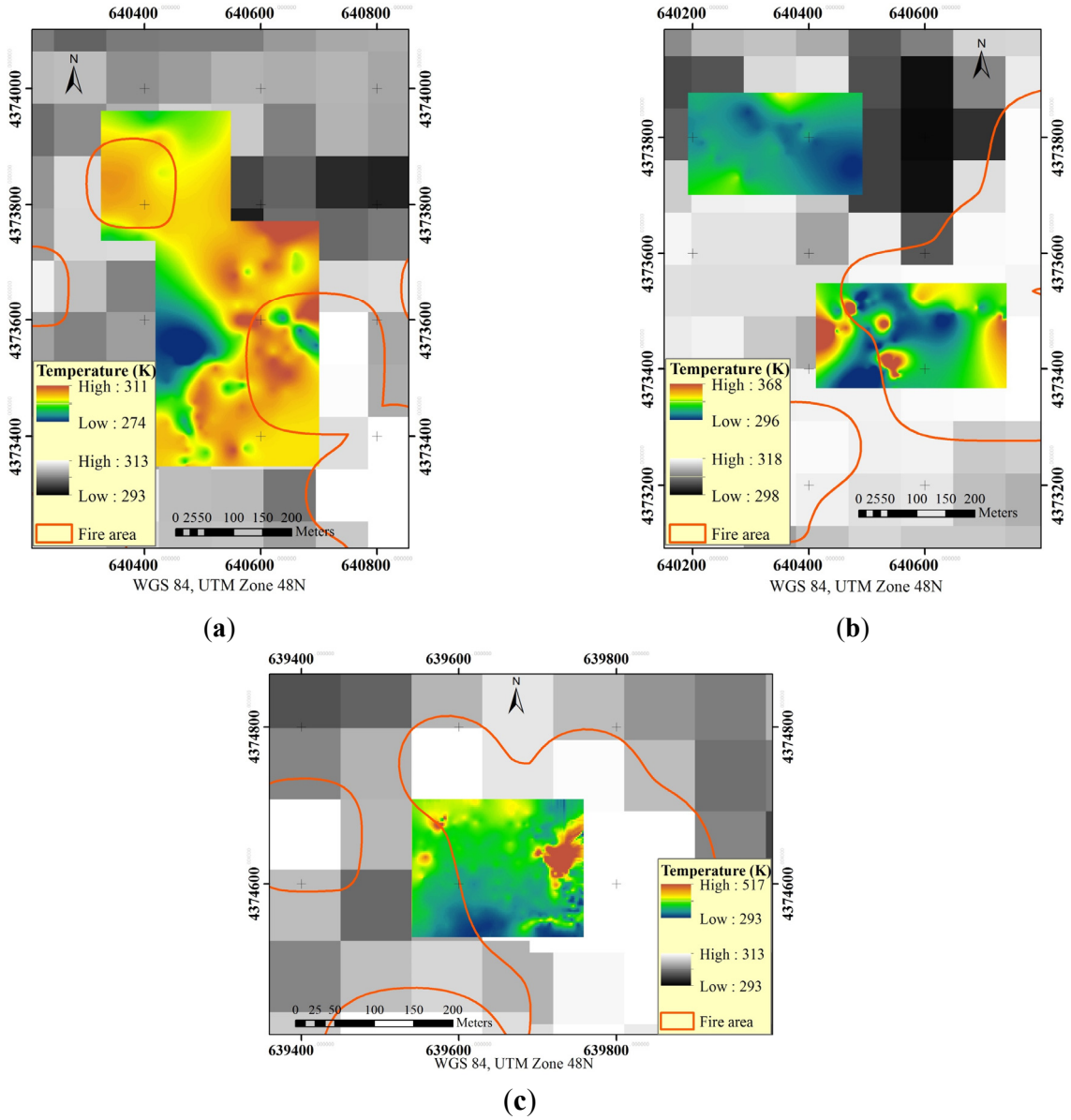

Figure 13. Coal fire polygons from SAGBT, overlaid on interpolated temperature measurements (color insets) for (**a**) 27 March 2013 and (**b**) 22 June 2013. A similar map (**c**) has SAGBT polygons for 27 March 2013 overlaid on interpolated measurements from 6 October 2013. ASTER TIR pixels are shown in gray.

4.6. Comparison between Coal Fires Retrieved from Images Acquired During Daytime, Nighttime and in Different Seasons

Coal fire areas retrieved from daytime-nighttime image pairs acquired on the same date were overlaid and compared (Figure 14). In addition, we addressed potential seasonal variability in fire identification by SAGBT by investigating fires detected in spring/fall, summer and winter. The daytime-nighttime image pair acquired in spring (Figure 14a) showed lower spatial agreement when compared to fire areas derived from summer (Figure 14b) or winter images (Figure 14c). A closer inspection of thermal anomaly values indicated increased anomalies during winter when the nighttime image was used (hypothesis test not shown). Fire areas identified by SAGBT in winter were 177.7 hm^2 (nighttime) and 145.7 hm^2 (daytime). The opposite was observed for image pairs acquired in summer and in spring/fall, as larger areas of coal fire were detected when daytime images were used. For the summer solstice image (22 June 2013), the daytime-derived fire area (154.8 hm^2) was 25.8% larger than the area for the nighttime image (123.1 hm^2). Differences were even larger in spring, when 29.7% more pixels of coal fires were identified using the daytime acquisition (251.7 hm^2), when compared to the nighttime image (194.0 hm^2). The observed variability can be explained by differences in thermal contributions from solar radiation. Due to reduced solar irradiation in winter, small areal differences are expected when daytime and nighttime images are used. As a result, increased sensitivity and more reliable detection of fires are expected for that season.

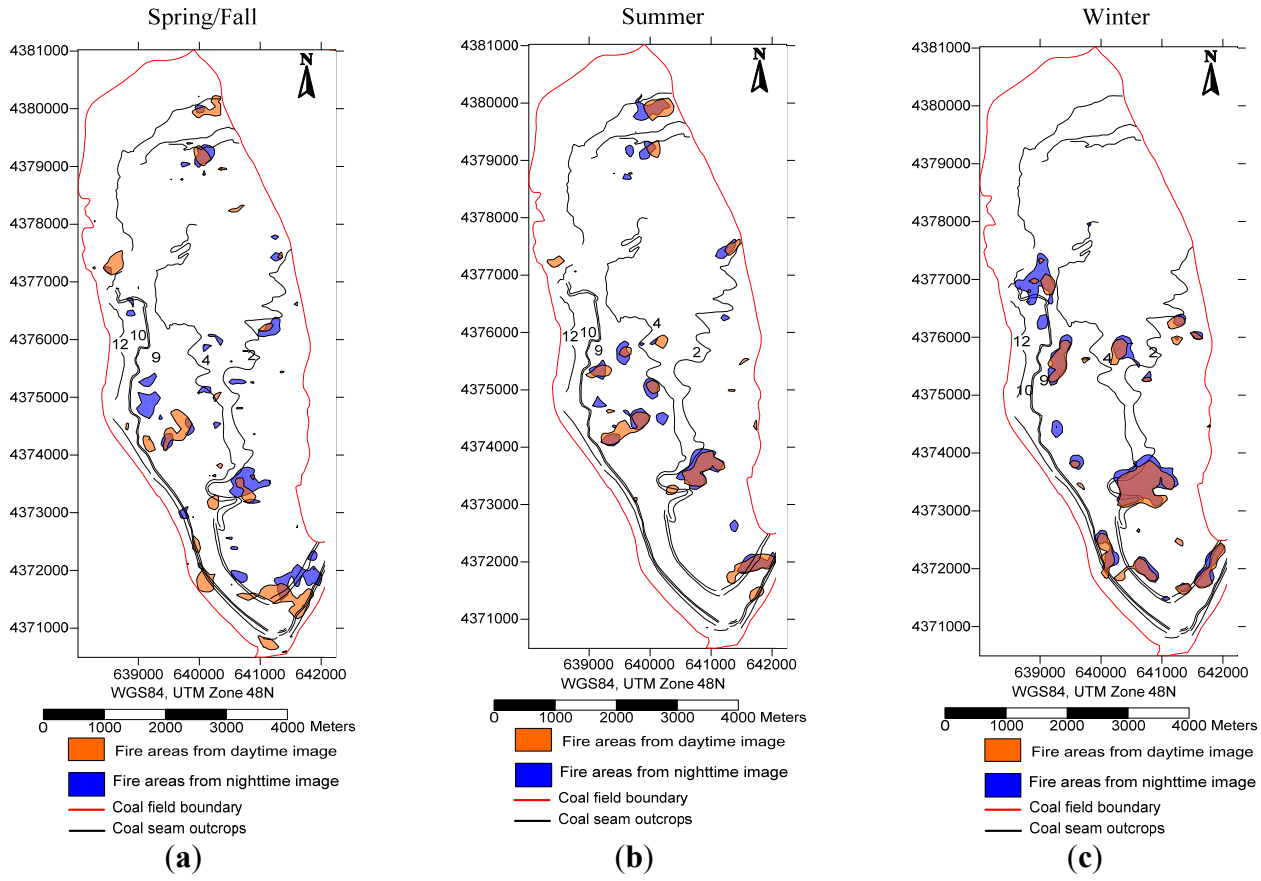

Figure 14. Coal fire areas retrieved from images acquired during daytime (orange areas) and nighttime (blue areas) for different seasons. Image pairs were acquired on (**a**) 27 March 2013; (**b**) 22 June 2013; and (**c**) 29 November 2007.

4.7. Comparison with Other Non-Interactive and in-situ Based Methods

To understand how SAGBT performs when compared to another non-interactive coal fire detection method, we compared the implementations of SAGBT and of the Moving Window algorithm used by [12–18]. Considering the importance of thermal anomaly identification and false positive rejection in coal fire detection, these steps were selected for method comparison. The Moving Window is an established method that incorporates two steps for anomaly identification and one step for false positive rejection. First, preliminary anomaly identification is used with moving windows of varied sizes to identify pixels that exceed a statistical threshold. This task differentiates anomaly pixels from the surrounding background. Then, during false positive rejection, adjacent thermally anomalous pixels are clustered based on cluster statistics (minimum, maximum, mean and standard deviation). The false positive elimination process in Moving Window uses previous knowledge of potential false positive patches to exclude large thermal anomalies, flat temperature areas, and small thermal anomalies. The second thermal anomaly identification step segments remaining thermal anomaly clusters using a cut-off percentage (70% or 85%) and delineates the final coal fires. SAGBT uses one step to identify thermal anomalies and one mechanism to reject false positives. Anomaly identification uses morphology thinning to skeletonize extreme gradient buffers to gradient lines, providing a self-adaptive thresholding to extract thermal anomalies. Thus, the method uses spatial thresholding to resolve temperature gradients associated with coal fires. In a relatively small and homogeneous coalfield, we used potential high temperature buffers and coalfield boundaries to limit the temperature reading scope of the thinned extremely gradient skeleton, which can be considered as a simple and implicit false positive elimination mechanism. Finally, the Moving Window method is driven by statistical attributes of coal fires, whereas SAGBT benefits from a computer graphics approach.

The shape and distribution of our coal fires are similar to results from studies using the Moving Window method. For example, the distribution of fine-tuned coal fires in the Wuda field mapped by Zhang [12] is similar to results shown in Figure 15a. Kuenzer *et al.* [14] and Wessling *et al.* [15] mapped coal fire surface anomalies in Wuda for 2003 using *in-situ* data and a combination of multiple coal fire related fields, expert knowledge and a Moving Window method based on thermal bands from Landsat. Our SAGBT-derived coal fires for September 2002 (Figure 15a) show similar distribution of thermal anomalies when compared to those results. The researchers in the study [16,17] delineated the coal fires in the Jharia coalfield in India by using Moving Window method, while it is incomparable to our results for the Wuda coalfield.

Reduced agreement was observed between SAGBT coal fires and results by *in-situ* methods and by approaches based on multiple fire-related factors [14,15,18]. For example, total coal fire areas for 2005 and for 2011 differ from results based on multi-spectral and panchromatic data from QuickBird reported by Kuenzer *et al.* [18]. For October 2005, we estimated a total coal fire area of 159.57 hm^2, compared to 112.96 hm^2 by the previous study. For 2010, results are closer as SAGBT identified 199.26 hm^2 of coal fires, against the reported 227.08 hm^2. Despite total area similarities, the shape of our coal fires (Figure 15b) differs from results for early 2010 in Kuenzer *et al.* [18]. This difference also exists when non-interactive methods based on satellite images and results from *in-situ* data are considered [15,18]. Differences most likely result from the definition of coal fires; one was based on comprehensive factors and human knowledge, and the other was mainly based on the thermal infrared

data and extracted by automatic algorithms. In addition, variability in coal fire identification is expected due to the use of images acquired in different dates and to different sensors.

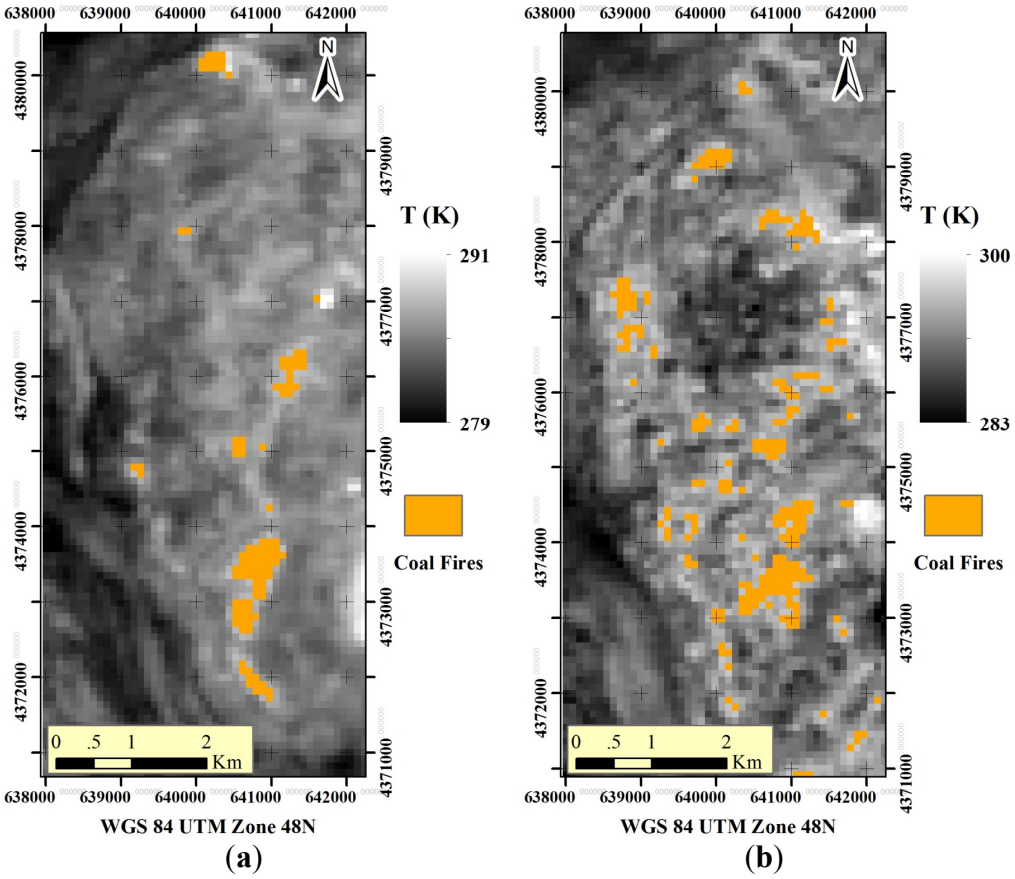

Figure 15. Coal fire areas retrieved from (**a**) nighttime images for 21 September 2002 and (**b**) daytime image for 26 March 2010. Coal fires were compared with results from literature.

SAGBT can mask subtle thermal anomalies associated with slow combustion in coal waste piles or coal storages, as shown by Figure 10a. Due to the lack of studies providing accuracy assessments, we make no claim that SAGBT was more accurate than the Moving Window and the field-based pixel-integrated methods [19]. For improving SAGBT results, we suggest partitioning the large area into relatively homogeneous small regions, considering their geological setting, geomorphology and land cover/use. As presented by [13], a fire risk map can be effectively used to mask out false coal fires. Future coal fire studies should incorporate statistical characterizations of potential thermal anomalies for false positive removal using orbital images and field measurements. Future studies could benefit from the incorporation of short wavelength infrared bands (e.g., from Landsat 8 or MODIS) and from derived band ratios, as these are presented by [16,17].

4.7. Uncertainty and Accuracy

Coal fires extracted by SAGBT divided the Wuda coalfield in high and low temperature areas (significance level = 0.05). The average spatial offset of SAGBT coal fires, calculated from measured fire spots, was 32.44 m and we estimate the positional error of our results to be less than 50% of an ASTER TIR pixel (< 45m). Our comparison between measured fire spots and coal fires from SAGBT

showed that approximately 70% of fire spots matched fire areas from ASTER images and that 87.5% of fire spots were within one-pixel distance from the coal fire areas. The ability of SAGBT to delineate fires using Landsat 8 TIRS data was also validated by coal fire spots. When TIRS data were used, 82.9% of the observed fire spots were within one-pixel from coal fire areas. A similar study by our group [20] showed that the majority of points (84.6%) were located within the detected fire area and that 97.5% of the points were within one-pixel buffers around these areas. Thus we estimate the matching rate between fire spots and SAGBT-derived coal fires to be in the 70%–85% range. SAGBT missed some weak or small coal fires, which were among the 14.8% observed fire spots missed by the algorithm. We infer that SAGBT did not perform well in detecting deep coal fires overlaid by thick rock strata, resulting from the weak heat signature of those fires.

5. Conclusions and Vision

The Self-Adaptive Gradient-Based Thresholding (SAGBT) method for coal fire detection proposed in our previous paper [8] was analyzed and validated. This satellite image-based method used ASTER thermal infrared images and relied on a coal fire risk area enclosed by the outer boundaries of coal-bearing strata to exclude false positives. To validate the SAGBT method, coal fires for nine different ASTER scenes were identified and compared in space and time. The analysis was based on two field campaigns in the Wuda coalfield, in China, which were conducted during satellite overpass on 27 March 2013 (spring equinox) and 22 June 2013 (summer solstice). Additional field measurements conducted on 6 October 2012 represented the fall season. Spring, summer, and fall images obtained from the ASTER sensor were analyzed together with more than 600 simultaneous surface temperature records. To match coarse TIR images to GPS points we used a two-step image registration procedure: "image-to-map" and "image-to-image". Image registration used GCPs of road intersections and thermal features (e.g., river turns, coal piles and lakes), resulting in errors of less than 45 m (less than half of an ASTER TIR pixel).

Comparison of delineated coal fires with field temperature measurements (points, lines and regions) and comparison of coal fire areas with thermal anomalies using sensors with different spectral, spatial and temporal resolutions showed the following:

(1) Extremely high gradient lines delineated by SAGBT generally agreed with coal fire boundaries in the field.
(2) A hypothesis test supported our prediction that coal fire boundaries can be used to segment the study site into a high-temperature coal fire area and a cold background, especially when coal fires from nighttime TIR images are used.
(3) About 70%–85% of observed coal fire sites matched coal fire areas from SAGBT. The average distance between fire sites and the nearest retrieved fire boundary (32.44 m) was less than half the pixel dimension (45 m). Approximately 15% of the observed fire spots were not identified by SAGBT.
(4) Coal fire areas from SAGBT match high-temperature pixels in the ASTER image, and the areas include the major extreme high-temperature regions derived from field samples.

(5) Similar spatial distribution in coal fire areas was observed for daytime and nighttime images, although differences in shape and size of areas occurred. Differences in area between daytime and nighttime acquisitions in spring were observed to be more dramatic than in the summer.

These results suggest that SAGBT has weak dependency on the accuracy of temperature retrieval, but the method depends strongly on the distribution of thermal features. Simultaneous observations by satellite and in the field offered an opportunity to validate a new proposed coal fire detection method.

Further research involving orbital remote sensing and simultaneous field measurements should focus on developing a solar radiation correction for daytime TIR images. A better understanding of the relationships between field temperatures, LST retrieved from daytime/nighttime satellite TIR images, and solar irradiation-induced temperature rise should assist in addressing the effects of solar heating on coal fire detection. In addition, measurements in fall and winter are expected to produce a four-season calibration of the gradient-based threshold method for coal fire detection. Finally, the SAGBT method can be applied to other TIR data, such as images from Landsat 8 TIRS and from the Moderate Resolution Imaging Spectroradiometer (MODIS) sensor. Applications of SAGBT can be extended to other fields, such as volcano monitoring, detection for forest and peat fires, and discovering for geothermal phenomena (hot springs, fumaroles, geysers, and mud pots) [21].

Acknowledgments

Funding for this work was provided by a Strategic Priority Research Program of the Chinese Academy of Sciences, Carbon Emission from Coal Spontaneous Combustion (Grant No. XDA05030200). The first author's visiting study at the University of Georgia (UGA) was sponsored by the China Scholarship Council. We thank Chunla He at UGA for improving the SAS scripts and analyses of the hypothesis test results. The authors wish to thank the anonymous reviewers for their constructive suggestions that improved the paper. Image acquisition was granted by the Land Processes Distributed Active Archive Center (LP DAAC) of the National Aeronautics and Space Administration (NASA), including the tasking of the ASTER orbital sensor to acquire images during field activities in China. ASTER images were accessed through the Earth Resources Observation Systems (EROS) Data Center of the U.S. Geological Survey (USGS).

Author Contributions

Xiaomin Du designed the research, defined image processing and data analysis approaches, processed images, analyzed data, interpreted results and wrote the manuscript. Sergio Bernardes defined image processing and data analysis approaches, interpreted results and wrote the manuscript. Daiyong Cao provided logistical support. Thomas R. Jordan scheduled image acquisition. Zhen Yan performed statistical analysis and developed software. Guang Yang and Zhipeng Li collected field data.

Conflicts of Interests

The authors declare no conflict of interest.

References

1. Gangopadhyay, P.K.; Maathuis, B.; Van Dijk, P. ASTER-derived emissivity and coal-fire related surface temperature anomaly: A case study in Wuda, North China. *Int. J. Remote Sens.* **2005**, *26*, 5555–5571.
2. Guney, M. Oxidation and spontaneous combustion of coal: Review of individual factors. *Colliery Guard.* **1968**, *216*, 105–110.
3. Cao, D.; Fan, X.; Guan, H.; Wu, C.; Shi, X.; Jia, Y. Geological models of spontaneous combustion in the Wuda coalfield, Inner Mongolia, China. *Rev. Eng. Geol.* **2007**, *18*, 23–30.
4. Zhang, J.; Kuenzer, C. Thermal surface characteristics of coal fires 1 results of *in-situ* measurements. *J. Appl. Geophys.* **2007**, *63*, 117–134.
5. Yan, G.; Mas, J.F.; Maathuis, B.; Xiangmin, Z.; Van Dijk, P. Comparison of pixel-based and object-oriented image classification approaches—A case study in a coal fire area, Wuda, Inner Mongolia, China. *Int. J. Remote Sens.* **2006**, *27*, 4039–4055.
6. Gautam, R.S.; Singh, D.; Mittal, A.; Sajin, P. Application of SVM on satellite images to detect hotspots in Jharia coal field region of India. *Adv. Space Res.* **2008**, *41*, 1784–1792.
7. Zhang X.; Van Genderen J.; Kroonenberg S. A method to evaluate the capability of Landsat-5 TM band 6 data for sub-pixel coal fire detection. *Int. J. Remote Sens.* **1997**, *18*, 3279–3288.
8. Du, X.; Cao, D.; Bernardes, S.; Jordan, J.; Yang, G.; Li, Z. Self-Adaptive gradient based thresholding method for coal fire detection using ASTER thermal infrared data, Part I: Methodology. *Remote Sens.* **2015**, Submitted.
9. Peng, S.; Zhang, J. *Coal Bearing Strata Sedimentary Environment and its Influence in the Wuda Coal Mining Area*; Mining Coal Industry Publishing House: Beijing, China, 1995. (In Chinese)
10. Zhang, J. *Underground Coal Fires in China: Origin, Detection, Fire-Fighting, and Prevention*; China Coal Industry Publishing House: Beijing, China, 2008, pp. 3, 43, 383. (In Chinese)
11. Gillespie, A.; Rokugawa, S.; Matsunaga, T.; Cothern, J.S.; Hook, S.; Kahle, A.B. A temperature and emissivity separation algorithm for advanced spaceborne thermal emission and reflection radiometer (ASTER) images. *IEEE Trans. Geosci. Remote Sens.* **1998**, *36*, 1113–1126.
12. Zhang, J. Spatial and Statistical Analysis of Thermal Satellite Imagery for Extraction of Coal Fire Related Anomalies. Ph.D. Thesis, Technical University Vienna, Vienna, Austria, 2004.
13. Kuenzer, C.; Zhang, J.; Li, J.; Voigt, S.; Mehl, H.; Wagner, W. Detecting unknown coal fires: Synergy of automated coal fire risk area delineation and improved thermal anomaly extraction. *Int. J. Remote Sens.* **2007**, *28*, 4561–4585
14. Kuenzer, C.; Zhang, J.; Hirner, A.; Bo, Y.; Jia, Y.; Sun, Y. Multitemporal *in-situ* mapping of the Wuda coal fires from 2000 to 2005—Assessing coal fire dynamics. In *Spontaneous Coal Seam Fires: Mitigating a Global Disaster. ERSEC Ecological Book Series*; UNESCO: Beijing, China, 2008; Volume 4, pp. 132–148.
15. Wessling, S.; Kuenzer, C.; Kessels, W.; Wuttke, M.W. Numerical modeling for analyzing thermal surface anomalies induced by underground coal fires. *Int. J. Coal Geol.* **2008**, *74*, 175–184.
16. Kuenzer, C.; Hecker, C.; Zhang, J.; Wessling, S.; Wagner, W. The potential of multidiurnal MODIS thermal band data for coal fire detection. *Int. J. Remote Sens.* **2008**, *29*, 923–944.

17. Hecker, C.; Kuenzer, C.; Zhang, J. Remote-sensing—Based coal-fire detection with low-resolution MODIS data. *Rev. Eng. Geol.* **2007**, *18*, 229–238.
18. Kuenzer, C.; Zhang, J.; Sun, Y.; Jia, Y.; Dech, S. Coal fires revisited: The Wuda coal field in the aftermath of extensive coal fire research and accelerating extinguishing activities. *Int. J. Remote Sens.* **2012**, *102*, 75–86.
19. Chatterjee, R. Coal fire mapping from satellite thermal IR data—A case example in Jharia coalfield, Jharkhand, India. *ISPRS J. Photogram. Remote Sens.* **2006**, *60*, 113–128.
20. Du X.; Cao D.; Yang G; Bernardes, S.; Li, S.; Li, F. Estimating Typical Four-Season Thermal Distribution and Self-Adaptive Gradient Based Thresholding Parameters over Coal Fire Areas in China Using Aster and Ldcm Tirs-A Case Study in the Wuda Coal Field, China, In Proceedings of the ASPRS 2014, Louisville, USA, 26 March 2014.
21. Kuenzer, C.; Guo, H.; Ottinger, M.; Zhang, J.; Dech, S. Spaceborne thermal infrared observation—An overview of most frequently used sensors for applied research. In *Thermal Infrared Remote Sensing*; Springer Science + Business Media: Dordrecht, Netherlands, 2013, pp. 131–148.